NANO LETTERS

2008
Vol. 8, No. 8
2131-2136

Electronic Transport through Ruthenium-Based Redox-Active Molecules in Metal−Molecule−Metal Nanogap Junctions

Ajit K. Mahapatro,[†] Jiewen Ying,[‡] Tong Ren,[‡] and David B. Janes*,[†]

Birck Nanotechnology Center, School of Electrical and Computer Engineering, Purdue University, West Lafayette, Indiana 47907, and Department of Chemistry, Purdue University, West Lafayette, Indiana 47907

Received November 15, 2007; Revised Manuscript Received January 23, 2008

ABSTRACT

Electronic transport through ruthenium-based redox-active organometallic molecules is measured by self-assembling diruthenium(III) tetra(2-anilinopyridinate)-di(4-thiolphenylethynyl) (*trans*-$Ru_2(ap)_4(C'CC_6H_4S-)_2$ (A) and *trans*- $Ru_2(ap)_4((C'CC_6H_4)_2S-)_2$ (B) molecules in nanogap molecular junctions. Voltage sweeps at a high scan rate show low bias current peaks (at $\pm 0.35 \pm 0.05$ V for A and $\pm 0.27 \pm 0.05$ V for B), which change to plateaus in slow bias scans and a second conductance peak at approximatley $\pm 1.05 \pm 0.15$ V. The peaks/plateaus are not observed in the return bias sweeps, possibly due to charge storage in the molecules. The energy states for the molecular orbitals of these molecules as estimated from the conductance peaks are in close agreement with the respective energy values from voltammetric measurements in solution.

Recent progress in molecular electronics, particularly single/few-molecule devices, is of great interest for future nanoelectronics.[1,2] Various organic molecules have been integrated into device structures to realize components such as rectifiers,[3] negative differential resistance (NDR),[4–8] bistable switches,[9–14] tunneling diodes, transistors,[15] logic-gates,[16] memory elements,[17] and sensors.[18,19] Most molecular electronic studies have employed systems (molecules plus contacts) in which the conduction is nonresonant, i.e., in which the molecular orbital energy levels are not aligned with the contact Fermi levels even under moderate applied biases.[20,21] In such systems, electrical transport measurements do not provide direct information about energy level alignments, and the molecule remains close to charge neutrality. There have been studies of molecular systems having redox-active side groups ($-NO_2$, $-NH_2$),[22] coordination complexes,[23,24] imino nitrogen ($-N=$) inserted in the backbone,[11,25] and functionalization with various headgroups ($-CN$, $-NO_2$, H_3CO_2C-, $-SH$).[22] These modified molecular complexes show various interesting electronic properties, including variations in the distance between the contact Fermi level and the closest molecular orbital, and Kondo effects associated with unpaired electrons. Also, some models attribute switching[11,25] and NDR[4] phenomena to redox events, typically along with a secondary process. Electronic conduction studies of redox-active molecules with suitable contacts can allow investigation of the energy-band alignments between the molecular levels and the contacts within the active device structure as well as studies of molecular species in specific charge states.

One approach that has proven useful for contacts suitable for single/few molecule measurements involves electromigration breaking of photolithographically defined gold (Au) microwires.[26] We have recently adopted these techniques to efficiently fabricate stable nanogap molecular junctions[23,27] (NMJs) for room temperature measurements. The NMJ structure has been used to measure the electronic properties of various organic[27,28] and biomolecular[29] species.

In this work, the electronic properties of diruthenium-containing redox-active organic molecules were studied in metal/molecule/metal (MMM) devices using the NMJ technique, and the molecular energy states were estimated and compared with the results from cyclic voltammogram measurements. Electrical transport measurements were performed through the NMJs containing diruthenium(III) tetra(2-anilinopyridinate)-di(4-thiolphenylethynyl), *trans*-$Ru_2(ap)_4(C'CC_6H_4S-)_2$ (**A**) and *trans*-$Ru_2(ap)_4((C'CC_6H_4)_2S-)_2$ (**B**) molecules (the molecular structures are sketched in Figure 1). Current peaks and plateaus were observed in current−voltage ($I-V$) characteristics during voltage scans from zero

* Corresponding author. Phone number: 1-765-494-9263. Fax number: 1-765-494-0811. E-mail address: janes@ecn.purdue.edu.

[†] Birck Nanotechnology Center, School of Electrical and Computer Engineering.

[‡] Department of Chemistry.

10.1021/nl072982c CCC: $40.75
Published on Web 06/27/2008

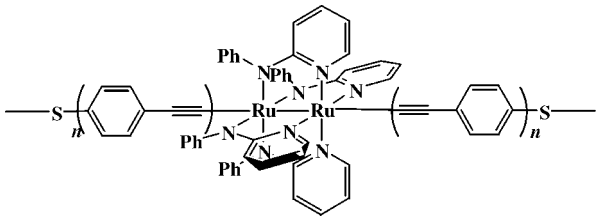

Figure 1. (a) Sketch of diruthenium molecular wires used in this study. Here $n = 1$ for molecule **A**, *trans*-$Ru_2(ap)_4(C{\equiv}CC_6H_4S-)_2$, and $n = 2$ for molecule **B**, *trans*- $Ru_2(ap)_4((C{\equiv}CC_6H_4)_2S-)_2$.

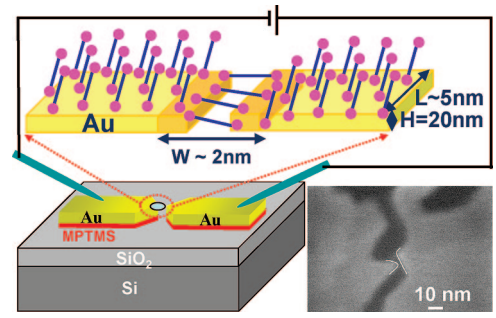

Figure 2. (a) Schematic of the device structure used in this study. Inset shows the molecular bridging at the nanogap region. (b) FESEM image of a sub-2-nm gap formed through an electromigration-induced break junction technique.

to higher bias (in both the positive and negative directions) at fast and slow scan rates, respectively. These features are absent in the return sweeps, i.e., while driving the bias back to zero. The positions of the molecular energy levels of highest occupied molecular orbital (E_{HOMO}) and lowest unoccupied molecular orbital (E_{LUMO}), with respect to the metal electrode Fermi-level (E_f) are estimated from the locations of the conductance peaks using the ideas of energy band alignment for MMM junctions with symmetric coupling at both metal/molecule contacts.[30] The estimated E_{HOMO} and E_{LUMO} values for both the diruthenium compounds (**A** and **B**) from the transport measurements are in close agreement with the energy values estimated from the voltammetric measurements in bulk solution.

The device engineering starts with the e-beam evaporation of 200 Å of Au on an oxidized silicon substrate coated with an organic adhesion monolayer of (3-mercaptopropyl)trimethoxysilane (MPTMS, purchased from Sigma-Aldrich, USA). The Au was lithographically patterned into microwires, each containing a notch at the center to localize the breaking position and connected to large area ($\sim 100 \times 100$ μm^2) pads for electrical probing in a microprobe station. The relatively stable nanogaps were formed by a room temperature electromigration breaking technique,[27] in which voltages are ramped across the Au microwires. The detailed experimental procedure and the chemical processes for Au layer deposition,[31] nanogap formation, and characterization[27] have been described earlier.[27,31] Before molecular deposition, the NMJ chips were plasma cleaned to remove any residual MPTMS or other organic contaminants from the gap region and rinsed with ethyl alcohol to remove the oxides from the Au layer, followed by rinsing the chip with the solvent, tetrahydrofuran (THF) and blowing dry with N_2 gas. The diruthenium compounds, *trans*-$Ru_2(ap)_4(C'CC_6H_4SCH_2CH_2SiMe_3)_2$ (**A′**, TMSE-**A**-TMSE) and *trans*-$Ru_2(ap)_4((C'C_6H_4)_2SCH_2CH_2SiMe_3)_2$ (**B′**, TMSE-**B**-TMSE), where trimethylsilyl ethylene (TMSE) $= -CH_2CH_2SiMe_3$, were prepared and characterized following the previously reported procedures.[32] For electrical transport experiments, the MMM junctions are formed by self-assembling the diruthenium-based molecules into the nanogaps using solution-based techniques. Here, a 2 mM THF solution of the Ru_2 compound was treated with a small amount of tetrabutylammonium fluoride (TBAF) to remove both of the TMSE protection groups from the original molecule (yielding **A** and **B**) in order to provide thiol end groups to bind to the Au nanoelectrodes. The NMJ chip was then exposed to the solution for 24 h in a N_2-purged glovebox. The chip was rinsed with the solvent (THF) to clean any residual ions from the molecule-bridged nanogap junctions. The physical situation of the NMJs following molecular deposition is sketched in Figure 2a. The electrical measurements were performed using a Hewlett-Packard 4156A precision semiconductor parameter analyzer. Cyclic voltammograms (CV) were recorded following previously described[32] measurement procedures using 0.20 M tetrabutylammonium hexaflurophosphate, $(n\text{-}Bu)_4NPF_6$, solution (THF, N_2-degassed) on a CHI620A voltammetric analyzer with a glassy carbon working electrode (3 mm diameter), a platinum (Pt)-wire auxiliary electrode, and a silver/silver chloride (Ag/AgCl) reference electrode for nonaqueous solution (Cypress). The concentration of diruthenium species was about 1.0 mM, and the ferrocenium/ferrocene couple was observed at 0.576 V under the experimental conditions.

Figure 2b presents a field emission scanning electron microscope (FESEM) image of a prototype nanogap junction with sub-2-nm length fabricated using room temperature electromigration breaking of the Au microwires. FESEM imaging and individual conductance values through the empty nanogap junctions are used to infer the gap length as well as the relative gap width. The general procedure is presented in our earlier work.[27] Prior studies of single/few organic molecules in electromigrated break junctions have typically involved deposition of the molecular species on the Au-microwires prior to electromigration, with the electromigration often performed at cryogenic temperature.[23] The current technique of fabricating nanogaps does not require cryogenic temperatures, is well suited for room temperature measurements, and allows characterization of the gap conductance prior to molecular deposition. For the room temperature electromigration technique, we have observed that the use of a molecular adhesion layer (MPTMS) beneath the Au allows a higher percentage of NMJs with sub-5-nm gaps ($\sim$ 25% for gap length of 1−2 nm and >40% for gap length of $\sim$5 nm, as estimated from the empty-gap conductance values) than can typically be achieved in Au-microwires with metallic (Ti, Cr) adhesion layers. The current technique also avoids leakage conduction paths, which can occur through metallic adhesion layers[26,33,34] or inherent cantilever effects in the case of hanging microwire[35,36] based NMJs. Electronic conduction through the molecules was

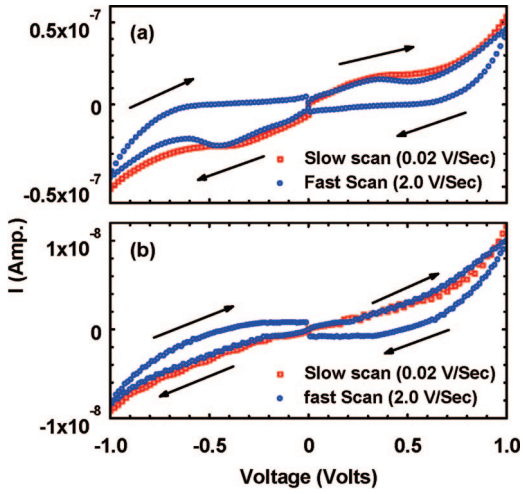

Figure 3. Room temperature $I-V$ characteristics through the nanogap MMM junctions containing (a) the molecule **A** and (b) the molecule **B**, showing curves measured at scan rates of 0.2 and 0.02 V/s, as indicated. The arrows indicate the direction of the voltage sweep for the respective portions of the curves. The current peak at low bias changes to a current step with a slow bias scan. These features are absent during return sweep to zero bias (i.e., scan from higher bias, both positive and negative direction to zero volt).

ensured by comparing the current levels through a given NMJ before and after localizing the specified molecular species. It has been observed that the NMJs with nanogap lengths comparable to the molecular lengths show enhancement in junction current after exposing the nanogap chip to the molecular solution. In the same chip, the NMJs with larger gap lengths ($>\sim$3 nm) do not show any enhancement in junction current after exposure to the molecular solution.

Parts a and b of Figure 3 show the $I-V$ characteristics measured through representative Au/**A**/Au and Au/**B**/Au NMJs, respectively. At least 10 devices were measured for each molecular species. On average, Au/**A**/Au NMJs show an initial low-bias conductance of $\sim(4.8 \pm 0.8) \times 10^{-8}$ S, while Au/**B**/Au NMJs show $\sim(5.5 \pm 0.5) \times 10^{-9}$ S. The stated uncertainties correspond to the maximum deviations observed over the set of measured devices. The higher conductance levels observed in the Au/A/Au devices suggest that molecule **A**, with a length of 2.1 nm, has less resistance than the 3.5 nm long molecule **B**, assuming comparable numbers of molecules, as will be discussed later. Although detailed calculations of conductance for these molecules is not available, this trend is consistent with the expected decrease in conductance values with increasing length.[37–40] Within a given device type, e.g., within the Au/**A**/Au devices, variations in the number of molecules bridging the nanogap, as well as variations in coupling strength at the S−Au contact,[41,42] may contribute to the observed spread in measured conductance values.

For the devices presented in Figure 3, the comparable empty-gap conductance values ($\sim$1 pS) through the nanogaps prior to the molecular depositions (molecule **A** and molecule **B**) indicate that both the NMJs are of comparable lengths ($\sim$1.5 nm). Normally, the electromigrated junctions provide a device structure involving single/few molecular species. Here, there is a possibility of bridging molecules between the electrodes within a small region in the nanogap in which the gap length (L) is comparable to molecular length. FESEM images of various nanogaps suggest that the region with $L \sim 2.0$ nm typically extends over a width of 2−3 nm. Since the molecules **A** and **B** are of diameters $\sim$1.3 nm, in the extreme case of a close-packed array of molecules bridging the nanogap region, there would be ca. 20 molecules of **A** or **B** bridging the gap in a NMJs. However, the packing densities of these molecules on a flat Au surface are significantly less than a monolayer; therefore the actual number of molecules in the gap is expected to be much less. Within the measured devices for a given molecular species, the current measurements do not show clear evidence of discrete levels of conductance, which would be expected if the conductance per molecule was uniform, given that it appears that each device contains a small integer number of molecules. As has been shown in prior studies which allow conduction measurements of a much larger number of devices,[43] significant spreads in conductance values are observed in nominally identical, single molecule devices. These spreads are attributed to variations in contact coupling or local molecule/contact geometry and likely explain the lack of clear conductance quantization in the present study. A systematic variation in the number of molecules within a gap (for **A** vs **B**) should contribute linearly to the junction conductance[44] but differences in surface coverage for the two species are not expected to be large enough to account for the difference in conductance in A vs B.

As shown in Figure 3a, the NMJ with molecule **A** exhibits a current peak at a low bias voltage (V_{peak}) for the scan performed at a scan rate of 2.0 V/s (fast scan). The observed current peak at $\sim\pm(0.32-0.45)$ V (varies from junction to junction) changed to a plateau (Figure 3a) when the sweep rate of the applied bias was reduced to 0.02 V/s (slow scan). This occurs at a voltage equivalent to V_{peak} and with a current level comparable to that observed at the peak in the fast scan. These features (peaks and plateau) are prominent during the scan toward higher voltages in both the positive and negative directions but are absent during return voltage sweeps to $V = 0$. The device is normally in a less conducting state during these return sweeps. Molecule **B** (Figure 3b) also exhibits the hysteresis, and a quasi-plateau is observed at a comparable voltage, although this effect is less prominent.

For the case of fast scans, where the voltage is swept from 0 to a voltage magnitude $\geq$1.0 V (positive or negative), and then immediately returned to zero, the hold time at $V = 0$ between the sweeps is typically a few seconds. A subsequent sweep in the opposite bias direction follows the high conductance state, indicating that the switching of conductance state (from high to low) was reversed during the hold period. Subsequent sweeps showed curves which are nominally the same as those reported in Figure 3 (including hysteresis) for the respective bias directions. For voltage sweeps in which the magnitude of the applied voltage is smaller than the peak voltage, V_{PEAK} (e.g., $<$0.2 V for devices with V_{PEAK} $\sim$0.35 V), hysteresis is not observed between the outbound (0 to $\pm V$) and return ($\pm V$ to 0) sweeps. For

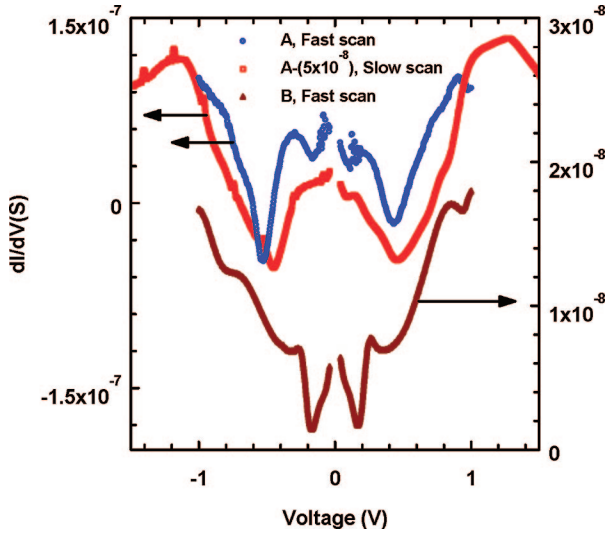

Figure 4. The d*I*/d*V* versus voltage plots for molecules **A** and **B**. Curves are shown for both fast and slow sweeps for molecule **A**, with the slow sweep covering a larger bias range. The slow sweep curve is offset vertically by -5×10^{-8} A for clarity. The peak voltage can be used to infer the position of the molecular HOMO and LUMO levels of the particular molecules with respect to the contact metal Fermi level.

the case of slow scans, comparable hysteresis and switching between conductance states are observed.

The conductance (G) as a function of voltage provides more clear signatures of the molecular levels, as well as a more direct comparison to typical theories. A peak in the $G-V$ relationship should correspond to the point at which the Fermi level of a contact is swept through a molecular level.[45] Curves representing the first derivative of the recorded $I-V$ characteristics (dI/dV vs V plot, using the Easy Plot scientific data analysis tool) are shown in Figure 4. During the scans toward higher voltages (0 to $\pm V$), conductance peaks are observed for both fast and slow bias scans. Conductance peaks were observed in a number ($\approx$10) of devices for each molecule, allowing determination of an average peak position and maximum deviation from the mean. Molecule **A** shows conductance peaks at $\pm 0.25 \pm 0.05$ V and $\pm 1.05 \pm 0.15$ V, and molecule **B** shows peaks at $\pm 0.265 \pm 0.05$ V and $\pm 0.77 \pm 0.08$ V. These features are absent in the return sweeps ($\pm V$ to 0). For the fast scans toward higher voltages, a negative differential resistance (conductance value becomes negative) behavior is observed starting at a bias of $\sim \pm 0.38 \pm 0.07$ V, for Au/**A**/Au devices, consistent with the observation of current peaks at comparable voltages in these devices. For the first 100−200 mV in each bias directions, the conductance for both molecular species initially decreases with increasing bias for the sweeps starting at $V = 0$. This decrease is also observed in subsequent sweeps, indicating that the effect does not correspond to a permanent change in device. The mechanisms responsible for this behavior are still under investigation.

The electronic properties of the NMJs depend mostly on the position of the highest occupied molecular orbital (HOMO) and lowest unoccupied molecular orbital (LUMO) with respect to the Fermi levels of the metal electrodes and the coupling strength at the metal/molecule contact. The low bias conductance is associated with the molecular density of states (DOS) near the Fermi level.[46] The observed peaks in the $G-V$ characteristics indicate the relative positions of the molecular orbital energy levels (E_{HOMO} and E_{LUMO}) in the respective molecules,[45] since the peaks are associated with the points at which the Fermi level of one contact passes through a molecular level.[45] In these systems, the coupling strengths at both the metal/molecule contacts play a key role in determining the electronic states of a molecule, which are generally broadened due to coupling to the contacts. The NMJs in the current work utilized Au−S covalent bonds at both the metal/molecule contacts. In this situation, the average electrostatic potential in the molecule (V_{mol}) is expected to be about half the applied voltage (V_{apl}),[30] i.e., the electrostatic potential difference V is divided between the two contact-to-molecule junctions with a voltage dividing factor, $\eta = V_{mol}/V_{apl} = 1/2$. For this case of comparable electrostatic coupling ($\eta = 0.5$), the observed conductance peak positions indicate the nearest energy states (either E_{HOMO} or E_{LUMO} levels) of the molecule. Two conductance peaks would appear for each HOMO or LUMO level, at bias voltages equal to $V_{peak} = \pm 2|E_{f(Au)} - E_{mol}|$, where E_{mol} stands for the molecular energy (E_{HOMO} or E_{LUMO}) and $E_{f(Au)}$ is the gold Fermi level. Therefore, the conductance peaks observed in molecule **A** at $V_{peak} = \pm 0.25 \pm 0.05$ V and $\pm 1.05 \pm 0.15$ V correspond to molecular energy levels located 0.13 and 0.53 eV away from $E_{f(Au)}$. On the basis of cyclic voltammetry (CV), which will be described in the following section, it appears that E_{HOMO} is closer to $E_{f(Au)}$ than is E_{LUMO}. Therefore, the energy levels observed in $G-V$ analysis can be identified as $|E_{f(Au)} - E_{HOMO}| \cong 0.13$ eV and $|E_{LUMO} - E_{f(Au)}| \cong 0.53$ eV. On the basis of the work function of Au, $E_{f(Au)} = 5.1$ eV with respect to the vacuum level (E_{vac}). Therefore, the inferred energy level positions with respect to E_{vac} are $E_{HOMO} = 5.23$ eV and $E_{LUMO} = 4.57$ eV for molecule **A**. Similarly, for molecule **B**, the observed conductance peaks at $\pm 0.265 \pm 0.05$ V and $\pm 0.77 \pm 0.08$ V correspond to $|E_{f(Au)} - E_{HOMO}| \cong 0.13$ eV and $|E_{LUMO} - E_{f(Au)}| \cong 0.38$ eV, which yield molecular energies of $E_{HOMO} = 5.23$ eV and $E_{LUMO} = 4.72$ eV, with respect to E_{vac}.

The molecular orbital energies of redox-active molecules can be estimated in the solution state using the CV technique. Figure 5 represents the CVs of both the diruthenium molecules **A′** and **B′** recorded versus a Ag/AgCl reference electrode in THF solution. For molecule **A′**, an oxidation peak was observed at +0.70 V and two reduction peaks were observed at −0.40 and −1.55 V. For molecule **B′**, an oxidation peak was observed at +0.74 V and two reduction peaks were observed at −0.33 and −1.5 V. The equivalent work function for a standard hydrogen electrode (SHE) in electrochemical experiments[47] is 4.43 eV. The potential of a Ag/AgCl reference electrode is 0.197 eV positive (+ve) with respect to the SHE potential, i.e, the $E_{Ag/AgCl} = 4.63$ eV. The above values, along with the observed oxidation (+0.7 V) and reduction (−0.4 and −1.55 V) peaks in the CV, yield molecular level energies of $E_{HOMO} = 5.33$ eV,

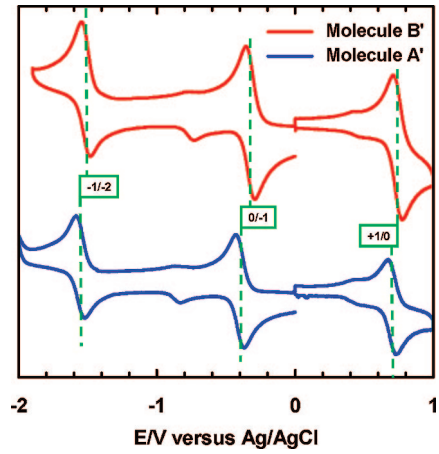

Figure 5. Cyclic voltammograms of the (a) **A′** and (b) **B′** molecules, measured with a Ag/AgCl reference electrode. The oxidation (0/+1) and reduction (0/−1 and −1/−2) states are labeled for both molecules.

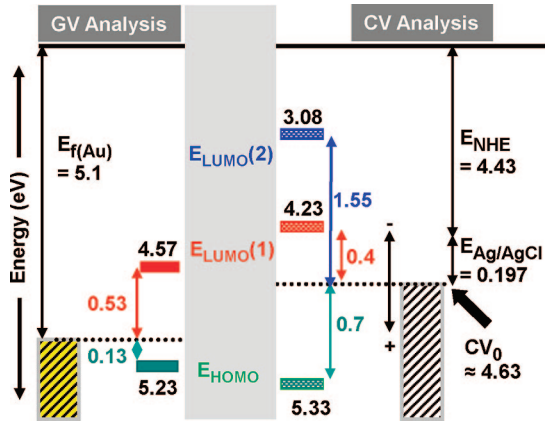

Figure 6. Molecular energy levels (HOMO and LUMO) of molecule **A** as inferred from the d*I*/d*V* (*G*−*V*) analysis (left side of figure) and CV measurements (right side of figure). The equivalent electrode work functions in the respective experimental setups have also been shown for comparison. The molecular level energies (E_{HOMO} and E_{LUMO}) were estimated from the oxidation and reduction peaks (in Figure 5) in CV measurements and from the peak positions in the *G*−*V* plot (in Figure 4).

E_{LUMO} = 4.23 eV, and E_{LUMO+1} = 3.08 eV for molecule **A**, all with respect to the vacuum level. A similar approach yields E_{HOMO} = 5.37 eV, E_{LUMO} = 4.3 eV, and E_{LUMO+1} = 3.13 eV for molecule **B′**.

The relative positions of E_{HOMO} and E_{LUMO} states are shown in Figure 6, as estimated from the electrical transport measurement (left side of figure) through molecule **A** and cyclic voltammetry experiments (right side of figure) on molecule **A′**, along with the Fermi levels of the respective electrodes. The good agreement for the molecular levels energies (within 0.1 eV (0.2 eV) for E_{HOMO} and 0.4 eV (0.4 eV) for E_{LUMO} for **A** (**B**)) between the energy values estimated from the peak positions in the *G*−*V* plot and oxidation and reduction peaks in CV measurements provides clear evidence of the respective molecular levels. The small differences in molecular levels estimated from the two techniques can be explained as some corrections due to solution versus solid state. The electrode potentials obtained from a solution voltammetric measurement generally agree with those measured for a surface-bound species;[48] therefore, changes in energy level positions associated with immobilization on the Au surface are expected to be modest. The same diruthenium molecules show retraceable oxidation and reduction peaks in solution phase CV measurements and hysteresis in *I*−*V* curves for forward and backward sweeps. This may be due to the presence of mobile ions to take the stored charge from the Ru complex during CV measurements. However, in the *I*−*V* measurements, neutralization of the stored charge would occur through the contacts, so the relatively localized nature of the charge states may result in storage times significantly different than the sweep times. The E_{LUMO+1} level could not be accessed in *I*−*V* measurements since the required bias (∼3.0 V) may destroy the S−Au contact or may change the electronic structure of the molecule due to the very high electric field through the NMJ.

The observed peaks/plateaus in *I*−*V* are likely due to charging events and can be assigned to HOMO/LUMO levels seen in CV measurements. The features in *I*−*V* and peaks in *G*−*V*/CV while passing through molecular energy levels are believed to be due to exchange of an electronic charge into or out of the molecular system. Retraceable (forward and backward voltage sweep) NDR peaks[4] and conductance switching[25] through the molecular systems indicate no charge storage in the molecular system while driving the voltage. In the current study, the hysteresis in *I*−*V* traces could be explained by the presence of a molecular state which becomes charged during the 0 to ±*V* sweep and remains charged during the return sweep. The charge storage is likely occurring at the localized molecular levels at the diruthenium complex, which is not well coupled to the contacts. Reported measurements through thiolates that contain redox capable metal centers of cobalt[23] and divanadium[24] have not observed charge storage effects, perhaps because the reported range of bias voltages is too low to access any molecular level or due to the fact that the metal complexes are spatially close to the metal electrodes, resulting in relatively strong coupling between the localized levels and the contacts. A sequential Coulomb blockade transport model,[49] which considers a trapping or localized level close to the E_{HOMO}, could explain the observed behavior. Charging of the localized level during a bias scan would shift the E_{HOMO} toward higher energy, resulting in a conductance and/or current peak. Provided that the level remains charged during the return bias sweep, a lower conductance trace without a peak is expected.

Density-functional theory (DFT) calculations on a comparable molecule,[50] $Ru_2(DMBA)_4(C_2Fc)_2$, suggest that the HOMO state consists of π-antibonding on Ru_2 and π-bonding between Ru and adjacent carbon, i.e., $\pi^*(Ru_2) + \pi(C{\equiv}C)$, with an energy of ∼4.8−5.0 eV (first oxidation at ∼+0.2 to +0.45 V). The LUMO state consists of δ-antibonding on Ru_2, i.e., $\delta^*(Ru_2)$, with an energy of ∼3.8−4.0 eV (first reduction at ∼−0.63 to −0.87 V). The π-orbital overlap on the central C≡C−Ru−Ru−C≡C backbone of the molecule should make the HOMO state relatively delocalized along

the NMJ. The LUMO is δ^* on the Ru−Ru part of the molecule and the adjacent carbons are off-set by 90° rotation to the d-orbitals of the Ru planes, making the LUMO state more localized in the direction orthogonal to current flow. The values inferred in the present study are in reasonable agreement with these values.

In conclusion, electronic conduction through diruthenium-based redox-active organometallic molecules (defined as **A** and **B** in Figure 1) were measured through a MMM device structure formed using an electromigration technique. The estimated molecular energy level values of E_{HOMO} and E_{LUMO} for the diruthenium molecules (**A** and **B**) using electrical transport measurements are in close agreement with the values inferred from CV measurements. This provides a tool to understand the location of the molecular energy levels with respect to the metal electrode Fermi levels. The current study demonstrates that devices employing redox-active molecules, in which the molecular levels are close to the metal Fermi level, allow resonant tunneling, along with observation of the molecules in specific charge states. The resulting devices could provide suitable structures for memory or chemical sensing applications.

Acknowledgment. This work was supported by NASA under Grant NCC 2-1363 and NSF/NER Award No. ECCS-0708582 to D.B.J. and NSF Grant No. CHE 0715404 to T.R. The authors thank Bhaskaran Muralidharan and Supriyo Datta for useful discussions.

References

(1) Joachim, C.; Gimzewski, J. K.; Aviram, A. *Nature* **2000**, *408*, 541–548.
(2) Nitzan, A.; Ratner, M. A. *Science* **2003**, *300*, 1384–1389.
(3) Aviram, A.; Ratner, M. *Chem. Phys. Lett.* **1974**, *29*, 277–283.
(4) Chen, J.; Reed, M. A.; Rawlett, A. M.; Tour, J. M. *Science* **1999**, *286*, 1550–1552.
(5) Le, J. D.; He, Y.; Hoye, T. R.; Mead, C. C.; Kiehl, R. A. *Appl. Phys. Lett.* **2003**, *83*, 5518–5520.
(6) Guisinger, N. P.; Basu, R.; Greene, M. E.; Baluch, A. S.; Hersam, M. C. *Nanotechnology* **2004**, *15*, S452−S458.
(7) Salomon, A.; Arad-Yellin, R.; Shanzer, A.; Karton, A.; Cahen, D. J. *J. Am. Chem. Soc.* **2004**, *126*, 11648–11657.
(8) Cai, L.; Cabassi, M. A.; Yoon, H.; Cabarcos, O. M.; McGuiness, C. L.; Flatt, A. K.; Allara, D. L.; Tour, J. M.; Mayer, T. S. *Nano Lett.* **2005**, *5*, 2365–2372.
(9) Emberly1, E. G.; Kirczenow, G. *Phys. Rev. Lett.* **2003**, *91*, 188301–188304.
(10) Collier, C. P.; Mattersteig, G.; Wong, E. W.; Luo, Y.; Beverly, K.; Sampaio, J.; Raymo, F. M.; Stoddart, J. F.; Heath, J. R. *Science* **2000**, *289*, 1172–1175.
(11) Gittins, D. I.; Bethell, D.; Schiffrin, D. J.; Nichols, R. J. *Nature* **2000**, *408*, 67–69.
(12) Donhauser, Z. J.; Mantooth, B. A.; Kelly, K. F.; Bumm, L. A.; Monnell, J. D.; Stapleton, J. J.; Price, D. W.; Rawlett, A. M.; Allara, D. L.; Tour, J. M.; Weiss, P. S. *Science* **2001**, *292*, 2303–2307.
(13) Blum, A. S.; Kushmerick, J. G.; Long, D. P.; Patterson, C. H.; Yang, J. C.; Henderson, J. C.; Yao, Y. X.; Tour, J. M.; Shashidhar, R.; Ratna, B. R. *Nat. Mater.* **2005**, *4*, 167–172.
(14) Chen, F.; He, J.; Nuckolls, C.; Roberts, T.; Klare, J. E.; Lindsay, S. *Nano Lett.* **2005**, *5*, 503–506.
(15) Cavallini, M.; Stoliar, P.; Moulin, J.-F.; Surin, M.; Lecle‘re, P.; Lazzaroni, R.; Breiby, D. W.; Andreasen, J. W.; Nielsen, M. M.; Sonar, P.; Grimsdale, A. C.; Mu1llen, K.; Biscarini, F. *Nano Lett.* **2005**, *5*, 2422–2425.
(16) Collier, C. P.; Wong, E. W.; Belohradský, M.; Raymo, F. M.; Stoddar, J. F.; Kuekes, P. J.; Williams, R. S.; Heath, J. R. *Science* **1999**, *285*, 391–394.
(17) Reed, M. A.; Chen, J.; Rawlett, A. M.; Price, D. W.; Tour, J. M. *Appl. Phys. Lett.* **2001**, *78*, 3735–3737.
(18) Janata, J.; Josowicz, M. *Nat. Mat.* **2002**, *2*, 19–24.
(19) McQuade, D. T.; Pullen, A. E.; Swager, T. M. *Chem. Rev.* **2000**, *100*, 2537–2574.
(20) Wang, W.; Lee, T.; Reed, M. A. *Phys. Rev.* **2003**, *B 68*, 035416–035422.
(21) Kushmerick, J. G.; Holt, D. B.; Yang, J. C.; Naciri, J.; Moore, M. H.; Shashidhar, R. *Phys. Rev. Lett.* **2002**, *89*, 086802–086805.
(22) Fan, F-R. F.; Yao, Y; Cai, L; Cheng, L; Tour, J. M; Bard, A. J. *J. Am. Chem. Soc.* **2004**, *126*, 4035–4042.
(23) Park, J.; Pasupathy, A. N.; Goldsmith, J. I.; Chang, C.; Yaish, Y.; Petta, J. R.; Rinkoski, M.; Sethna, J. P.; Abruna, H. D.; McEuen, P. L.; Ralph, D. C. *Nature* **2002**, *417*, 722–725.
(24) Liang, W.; Shores, M. P.; Bockrath, M.; Long, J. R.; Park, H. *Nature* **2002**, *417*, 725–729.
(25) He, J.; Fu, Q.; Lindsay, S.; Ciszek, J. W.; Tour, J. M. *J. Am. Chem. Soc.* **2006**, *128*, 14828–14835.
(26) Park, H.; Lim, A. K. L.; Alivisatos, A. P.; Park, J.; McEuen, P. L *Appl. Phys. Lett.* **1999**, *75*, 301–303.
(27) Mahapatro, A. K.; Ghosh, S.; Janes, D. B. *IEEE Trans. Nano Tech.* **2006**, *5*, 232–236.
(28) Mahapatro, A. K.; James, D. B. *J. Nanosci. Nanotechnol.* **2007**, *7*, 2134−2138.
(29) Mahapatro, A. K.; Jeong, K. J.; Lee, G. U.; Janes, D. B. *Nanotechnology* **2007**, *18*, 195202.
(30) Datta, S.; Tian, W.; Hong, S.; Reifenberger, R.; Henderson, J. I.; Kubiak, C. P. *Phys. Rev. Lett.* **1997**, *79*, 2530–2533.
(31) Mahapatro, A. K.; Scott, A.; Manning, A.; Janes, D. B. *Appl. Phys. Lett.* **2006**, *88*, 151917–151919. Mahapatro, A. K.; Mallick, G.; Joyner, K.; Zheng, Q. D.; Prasad, P. N.; Karna, S. P.; Janes, D. B. Unpublished.
(32) Ren, T.; Parish, D. A.; Xu, G-L.; Moore, M. H.; Deschamps; J. R.; Ying, J-W.; Pollack, S. K.; Schull, T. L.; Shashidhar, R. *J. Organomet. Chem.* **2005**, *690*, 4734–4739.
(33) Yu, L. H.; Natelson, D *Nano Lett.* **2000**, *0*, A−E.
(34) Bolotin, K. I.; Kuemmeth, F.; Pasupathy, A. N.; Ralph, D. C. *Appl. Phys. Lett.* **2004**, *84*, 3154–3156.
(35) Reichert, J.; Ochs, R.; Beckmann, D.; Weber, H. B.; Mayor, M.; Löhneysen, H. v *Phys. Rev. Lett.* **2002**, *88*, 176804.
(36) Kergueris, C.; Bourgoin, J.-P.; Palacin, S.; Esteve, D.; Urbina, C.; Magoga, M.; Joachim, C. *Phys. Rev. B* **1999**, *59*, 12505–12513.
(37) Asi, Y.; Fukuyama, H. *Phys. Rev. B* **2005**, *72*, 085431.
(38) Pauly, F.; Viljas J. K.; Cuevas, J. C. *arXive:0709.3588*, 2007.
(39) Samanta, M. P.; Tian, W.; Datta, S.; Henderson, J. I.; Kubiak, C. P. H. *Phys. Rev. B* **1997**, *53*, R7626−R7629.
(40) Venkataraman, L.; Klare, J. E.; Nuckolls, C.; Hybertsen, M. S.; Steigerwald, M. L. *Nature* **2006**, *442*, 904–907.
(41) Li, X.; He, J.; Hihath, J.; Xu, B.; Lindsay, S. M.; Tao, N. J. *J. Am. Chem. Soc.* **2006**, *128*, 2135–2141.
(42) Grigoriev, A.; Sköldberg, J.; Wendin, G.; Crljen, Z. *Phys. Rev. B* **2006**, *74*, 045401.
(43) Xu, B. Q.; Tao, N. J. *Science* **2003**, *301*, 1221–1223.
(44) Kushmerick, J. G.; Naciri, J.; Yang, J. C.; Shashidhar, R. *Nano Lett.* **2003**, *3*, 897–900.
(45) Tian, W.; Datta, S.; Hong, S.; Reifenberger, R.; Henderson, J. I.; Kubiak, C. P. *J. Chem. Phys.* **1998**, *109*, 2874–2882.
(46) Datta, S. *Electron transport in mesoscopic systems*; Cambridge University Press: Cambridge, 1995.
(47) Reiss, H.; Heller, A. *J. Phys. Chem.* **1985**, *89*, 4207–4213.
(48) Chidsey, C. E. D. *Science* **1991**, *251*, 919–922.
(49) Muralidharan, B.; Mahapatro, A. K.; Janes, D. B. Datta, S. (Unpublished).
(50) Xu, G.-L.; Crutchley, R. J.; DeRosa, M. C.; Pan, Q.-J.; Zhang, H.-X.; Wang, X.; Ren, T. *J. Am. Chem. Soc.* **2005**, *127*, 13354–13363.

NL072982C